Microscopy and Microanalysis (2022), **28**, 227–242
doi:10.1017/S1431927621013763

Microscopy AND Microanalysis

Original Article

Response of Olfactory Sensory Neurons to Mercury Ions in Zebrafish: An Immunohistochemical Study

Maurizio Lazzari*†, Simone Bettini†, Liliana Milani, Maria G. Maurizii and Valeria Franceschini
Department of Biological, Geological and Environmental Sciences, University of Bologna, Bologna 40126, Italy

Abstract

Olfactory sensory neurons (OSNs) of fish belong to three main types: ciliated olfactory sensory neurons (cOSNs), microvillous olfactory sensory neurons (mOSNs), and crypt cells. Mercury is a toxic metal harmful for olfaction. We exposed the olfactory epithelium of zebrafish to three sublethal Hg^{2+} concentrations. Molecular markers specific for the different types of OSNs were immunohistochemically detected. Image analysis of treated sections enabled counting of marked cells and measurement of staining optical density indicative of the response of OSNs to Hg^{2+} exposure. The three types of OSNs reacted to mercury in a different way. Image analysis revealed that mOSNs are more susceptible to Hg^{2+} exposure than cOSNs and crypt cell density decreases. Moreover, while the ratio between sensory/nonsensory epithelium areas is unchanged, epithelium thickness drops, and dividing cells increase in the basal layer of the olfactory epithelium. Cell death but also reduction of apical processes and marker expression could account for changes in OSN immunostaining. Also, the differential results between dorsal and ventral halves of the olfactory rosette could derive from different water flows inside the olfactory chamber or different subpopulations in OSNs.

Key words: crypt cells, immunohistochemistry, mercury ions, olfactory epithelium, olfactory sensory neurons, zebrafish

(Received 22 July 2021; revised 1 November 2021; accepted 10 November 2021)

Introduction

Inside the olfactory chamber, the olfactory sensory neurons (OSNs) of fish are directly exposed to water and its pollutants, which can interact with the dendritic terminations, affecting their integrity and functions (Sorensen & Caprio, 1998; Laberge & Hara, 2001; Zielinski & Hara, 2006; Tierney et al., 2010; Azizishirazi et al., 2014; Lari et al., 2019). In the olfactory mucosa covering the olfactory lamellae of fish olfactory rosette, morphologically and biochemically distinct types of OSNs are present (Hansen et al., 2003; Zielinski & Hara, 2006): ciliated olfactory sensory neurons (cOSNs) and microvillous olfactory sensory neurons (mOSNs), common to all vertebrates (Eisthen, 1992; Zielinski & Hara, 2006), and the crypt cells, exclusively described in cartilaginous, Polypteriformes, and teleost fish (Hansen & Finger, 2000; Ferrando et al., 2006, 2007, 2011). Axons emerging from OSNs converge in the olfactory nerves that innervate the glomerular layer of the olfactory bulbs (Hamdani & Døving, 2007). Olfactory sensory neurons have different signaling pathways, so different pollutants could be selective in their effects, causing changes in the response of OSNs to specific odors (Dew et al., 2014, 2016).

In aquatic ecosystems, heavy metals are common anthropogenic pollutants, persistent, and toxic at very low concentrations (Azizishirazi et al., 2014). They can cause histopathological (Bettini et al., 2006*a*, 2006*b*; Tierney et al., 2010; Lazzari et al., 2017, 2019) and functional (McIntyre et al., 2008; Tierney et al., 2010; Dew et al., 2012, 2014, 2016; Hentig & Byrd-Jacobs, 2016; Razmara et al., 2021) alterations to the olfactory system of fish, affecting various behaviors guided by olfaction, such as food searching, recognition of sexual partners, alarm cue, and predators avoidance (Scott et al., 2003; Sandahl et al., 2007; McIntyre et al., 2012; Azizishirazi et al., 2014; Abreu et al., 2016, 2017; Hentig & Byrd-Jacobs, 2016).

Mercury is a global, bio-accumulative persistent and toxic metal, which causes a very high risk to environmental and human health (for references, see Bernhoft, 2012; Syversen & Kaur, 2012; Bjørklund et al., 2017; Ha et al., 2017; Zhu et al., 2018). It is present in the environment in consequence of both natural processes (volcanic events, forest fires, rock weathering) and human activities (Risher & De Rosa, 2007). Anthropogenic sources include sources of nonoccupational exposure before mercury was replaced with safe substances (home, office, school, and health care devices: thermometers, barometer, sphygmomanometers, fluorescent bulbs, batteries, paints, inks), fossil fuel combustions, and occupational exposures (dental practice, mining activities, various industrial applications) (Bhan & Sarkar, 2005; Risher & De Rosa, 2007). Mercury exists in three chemical forms: elemental mercury, known as metallic mercury, organic mercury, mainly methyl mercury, and inorganic mercury compounds, mercury salt, mainly mercuric chloride. Each is characterized by a specific profile of toxicity (Guzzi & La Porta, 2008). In addition to elemental mercury which is slightly water soluble

***Corresponding author:** Maurizio Lazzari, E-mail: maurizio.lazzari@unibo.it
†The first two authors contributed equally to this work.

Cite this article: Lazzari M, Bettini S, Milani L, Maurizii MG, Franceschini V (2022) Response of Olfactory Sensory Neurons to Mercury Ions in Zebrafish: An Immunohistochemical Study. *Microsc Microanal* **28**, 227–242. doi:10.1017/S1431927621013763

and represents only a small portion of the total mercury in superficial freshwater, inorganic mercury together with organic mercury are the chemical forms primarily found in water, sediment, soil, and living organisms (Zhu et al., 2018). In water, both inorganic and organic mercury are found in dissolved, colloidal, and suspended phases. In nature, the different mercury chemical forms undergo complex cycling and transformations (Krabbenhoft & Rickert, 1995; Gonzalez-Raymat et al., 2017). Several environmental models for mercury transport and fate in aquatic systems have been developed, which represent valuable decision-making tools in mercury pollution control and management (see Zhu et al., 2018). Due to mercury ubiquitous environmental presence, freshwater and seawater fish may contain large amounts of it taken through the food chain. That is why eating large amounts of fish is hazardous especially for children and the developing fetus in pregnant women (Goldman & Shannon, 2001).

Mercury is a diffuse neurotoxic agent affecting fish olfaction: in the Atlantic salmon, it was observed accumulation of mercuric chloride around the borders of OSNs (Tierney et al., 2010), while it caused cilia degeneration and cell death (both sensory and non-sensory) in the Indian major carp after extended exposure (15 and 30 days) to sublethal doses (Ghosh & Mandal, 2014). Unlike copper (Razmara et al., 2021), the mechanisms by which mercury affects olfaction are less known (Ribeiro et al., 1995). Indeed, nothing is reported about behavioral responses or adverse effects after short-term exposure (less than 7 days) in adult fish, so it is impossible to compare mercury effects with other metal toxicity.

In this study, we analyzed the effect of exposure to sublethal doses of mercury ions (Hg^{2+}) in the three different types of OSNs in zebrafish (*Danio rerio* Hamilton, 1882). Zebrafish is a suitable model because immunohistochemical properties of its olfactory organ are extensively described in the literature (Hill et al., 2005; Germanà et al., 2007; Gayoso et al., 2011; Braubach et al., 2012), and, moreover, we can compare mercury data with those concerning other metals (Lazzari et al., 2017, 2019).

Materials and Methods

Animals

The study was performed on 40 adult zebrafish. Fish of both sexes, ~6 months old and about 4 cm long were purchased from the Coral Aquarium, Bologna, Italy. They were acclimatized in tanks filled with a 1:2 mixture of dechlorinated tap and distilled water for 30 days, at 25°C in a 12:12 light–dark cycle. Automatic fish feeders distributed commercial food twice a day. All procedures were in accordance with the guidelines of European Communities Council Directive (86/609/CEE), the current Italian legislation regarding the use and care of animals, and the guidelines issued by the US National Institutes of Health. This study was approved by the Scientific Ethics Committee of the University of Bologna (protocol no. 17/79/2014).

Mercury Exposure

Cruz et al. (2013) listed some studies reporting the mercury concentration of 20 μg/L found in the aquatic environment. In their study on zebrafish larvae, Sun et al. (2018) applied the environmentally relevant concentration of 16 μg/L Hg^{2+}. In the present study, we decided to use Hg^{2+} concentrations based on the lethal concentration 50 (LC_{50}) and not possible environmental values because they have a large range of variability (see Fleck et al., 2016 for an estimation of the total concentration of mercury in different aquatic sites in Western North America). In the US EPA ECOTOX database (http://cfpub.epa.gov/ecotox/), LC_{50} for mercury chloride measured in adult zebrafish (6-month old) after 48 h exposure is >60–100 μg/L (Bresch, 1982). In the present study, we used three Hg^{2+} concentrations made from mercuric chloride (Merck, Darmstadt, Germany) dissolved in acclimatization water: two concentrations were supposed to be sublethal: low quantity (LQ), 0.25 μM of mercuric chloride, corresponding to 50 μg/L of Hg^{2+}; medium quantity (MQ), 0.5 μM of mercuric chloride, corresponding to 100 μg/L of Hg^{2+}. The third concentration was over the LC_{50} range found by Bresch (1982) and Wang et al. (2013*a*): high quantity (HQ), 1 μM of mercuric chloride, corresponding to 200 μg/L of Hg^{2+}. However, Ung et al. (2010) determined that a 4-day exposure to 300 μg/L of mercuric chloride (~220 μg/L of Hg^{2+}) induces mortality in less than 50% of adult zebrafish (30%). Due to a certain discrepancy in lethal values in literature (Vutukuru & Basani, 2013; Wang et al., 2013*a*; Macirella et al., 2016; Amorim et al., 2017), we decided to take into account also the concentration of 1 μM $HgCl_2$. Each of three 10 L tanks containing 50, 100, and 200 μg/L of Hg^{2+} respectively, housed 10 fish. According to a static/renewal system, fish were moved to new tanks containing freshly prepared Hg^{2+} solutions every 24 h. The effect of the three concentrations of Hg^{2+} on olfactory mucosa was evaluated in fish sacrificed after 4-day (96 h) exposure, according to standard procedure in acute toxicity tests. Ten control fish were hosted in a tank containing acclimatization water, changed every 24 h. Control animals were sacrificed at the same time as mercury-exposed fish. Table 1 reports representative values of water parameters for acclimatization, treatment, and control tanks.

Tissue

Zebrafish, previously anesthetized with 0.1% 3-aminobenzoic acid ethyl ester (MS-222, Sigma, St. Louis MO, USA), were sacrificed by decapitation. Brains were exposed after dorsal cranium removal. Heads were fixed by immersion in a modified Bouin's fixative solution (see Lazzari et al., 2019) for 24 h at room temperature. After multiple extended 0.1 M phosphate buffer washes, specimens were decalcified in 0.25 M buffered EDTA, pH 7.4, for 9 days at room temperature, dehydrated, and then embedded in Paraplast Plus (Leica Biosystems, Richmond, IL, USA; melting point 55–57°C). Five μm-thick serial frontal sections were collected on silanized slides (Sigma). Some sections were colored with hematoxylin and eosin. Immunohistochemical detection was carried out on adjacent slides.

Immunohistochemistry

Details of the method are reported in Lazzari et al. (2017). Briefly, sections were deparaffinized, rehydrated, immersed in 1% H_2O_2 for endogenous peroxidase blocking, and incubated separately with six primary antibodies, in a moist chamber on an orbital shaker at 4°C, overnight: (a) rabbit polyclonal anti-calretinin (AB5054; Chemicon International, Temecula, CA, USA; used dilution 1:1,000), which in zebrafish detects a heterogeneous population of ciliated and microvillous olfactory neurons (Bettini et al., 2016); (b) rabbit polyclonal anti-$G_{\alpha\ olf}$ (sc-385; Santa Cruz Biotechnology, Santa Cruz, CA, USA; used dilution 1:500), which is specific for ciliated olfactory neurons (Gayoso et al., 2011; Braubach et al., 2012); (c) rabbit

https://doi.org/10.1017/S1431927621013763 Published online by Cambridge University Press

Table 1. Water Parameters of Acclimation, Control, and Hg^{2+} Exposure Tanks.

	NO_3 mg/L	NO_2 mg/L	GH dH	KH dH	pH
Acclimation tanks, new water, before fish insertion	<25	<0.5	14–21°	10	7.4–7.5
Acclimation tanks, after 24 h fish presence, before water change	<25	<0.5	14–21°	10	7.3–7.4
Control tanks, new water, before fish insertion	<25	<0.5	14–21°	10	7.4–7.5
Control tanks, after 24 h fish presence, before water change	<25	<0.5	14–21°	10	7.3–7.4
Exposure tanks, new water, before fish insertion	<25	<0.5	14–21°	10	7.4–7.5
Exposure tanks, after 24 h fish presence, before water change	<25	<0.5	14–21°	10	7.3–7.4

dH, degree of hardness; GH, general hardness; KH, carbonate hardness.

polyclonal anti-transient receptor potential cation channel, subfamily C, member 2 (anti-TRPC2; LS-C95010; LifeSpan BioSciences, Seattle, WA, USA; used dilution 1:200), a marker for microvillous olfactory neurons (Bettini et al., 2016); (d) rabbit polyclonal anti-tyrosine protein kinase A (anti-TrkA; sc-118; Santa Cruz Biotechnology; used dilution 1:100), which marks olfactory crypt cells in zebrafish (Ahuja et al., 2013; Bettini et al., 2016); (e) mouse monoclonal anti-human neuronal protein HuC/HuD (anti-HuC/D; Clone 16A11; A-21271; Molecular Probes, Eugene, OR, USA; used dilution 1:100), a nuclear marker of immature and mature neurons (Iqbal & Byrd-Jacobs, 2010; Bettini et al., 2016); (f) monoclonal mouse anti-proliferating cell nuclear antigen (anti-PCNA; Clone PC10; P 8825; Sigma; used dilution 1:500), which detects dividing cells (Iqbal & Byrd-Jacobs, 2010; Bettini et al., 2016). Anti-TRPC2 is specifically developed against zebrafish antigens. All the other antibodies here applied were previously successfully tested on zebrafish olfactory organs by other authors. The sections were incubated in the secondary antibody for 1 h 30 min at room temperature: HRP-conjugated goat anti-rabbit IgG (PI-1000; Vector Laboratories, Burlingame, CA, USA; used dilution 1:100) for polyclonal primary antibodies, and HRP-conjugated goat anti-mouse IgG (A4416; Sigma; used dilution 1:100) for the monoclonal primary antibody. The immunoreaction was revealed with 0.1% 3,3-diaminobenzidine (DAB; Sigma) as substrate. Sections from untreated fish served as positive controls. Negative controls for the specificity of the immunostaining consisted in exclusion of primary antibodies replaced with 3% normal goat serum.

Image Acquisition, Quantification, and Statistical Analysis

Except for PCNA, only sensory areas of the lamellae were sampled. Comparisons between fish were made selecting central lamellae from similar sections of the olfactory organ as it appears in frontal sections of the head (Fig. 1). Bright-field images of the olfactory organ were taken using an Olympus BH-2 microscope (Olympus Italia, Segrate, Italy) equipped with a BEL BlackL 5,000 digital camera (BEL Engineering, Monza, Italy). Light conditions were the same throughout acquired images. Micrographs were assembled with Adobe Photoshop CS3 (Adobe Systems, San Jose, CA, USA). Image processing was realized without content alteration. ImageJ 1.52o software (https://imagej.nih.gov/ij/) was employed in measurements of sensory lamellae. In anti-calretinin immunostained sections, the thickness was measured from the epithelial basal lamina to the apical surface, excluding cilia and microvilli. Both labeling pattern and the presence of long cilia on the surface of nonsensory areas were used as characteristics to distinguish between sensory and nonsensory epithelial areas. We measured the areas (μ^2) covered by sensory and nonsensory epithelia in three lamellae per section using ImageJ 1.52o software, then we calculated and averaged the ratios of sensory to nonsensory epithelium areas.

A physical disector method was applied for evaluating the densities of TrkA-positive cells (Bettini et al., 2016) and PCNA-positive cells. Proliferating cells were counted in the central rosette, from the interlamellar curves to the sensory/nonsensory borders of each lamella (Fig. 1), while the outer region was not considered, being not involved in neurogenesis (Bayramli et al., 2017). Anti-$G_{\alpha\ olf}$, anti-TRPC2, and anti-HuC/D immunostaining patterns did not permit cell discrimination and counting (see also Bettini et al., 2016; Lazzari et al., 2017, 2019), so we evaluated the Optical Density (OD) since the immunostaining intensity can be considered as an indirect index of the number of immunopositive cells (Iqbal & Byrd-Jacobs, 2010). In olfactory lamellae, average gray values of sensory regions and background-unstained zones were obtained by ImageJ analysis. The OD was then calculated as the logarithm of the ratio between gray values of background and sensory Region Of Interest.

In all measurements, data were obtained and averaged from three lamellae per section. For each antibody tested, mean values of fish groups were compared by ANOVA and LSD post hoc test. Using Excel 2016 (Microsoft Corporation, Redmond, WA, USA), bar graphs of mean values ± standard errors were obtained.

Results

Exposure of zebrafish to the highest Hg^{2+} ion concentration for 96 h caused one fish death out of a sample of ten. At the highest concentrations, the only appreciable micro-anatomical/histological effect was an increase in the unicellular mucous glands opening onto the luminal surface of the olfactory lamellae (Fig. 2). Instead, tissue disruption and metaplasia were not detected in the olfactory lamellae that also maintained their spatial arrangement. Olfactory rosettes retained their morphology. In hematoxylin eosin-stained sections, light microscopy analysis of the lamellae with high magnification revealed that even the highest mercury concentration applied did not cause removal or significant reduction of cilia (Fig. 3).

Incubation with anti-calretinin antibody that stains cell bodies and dendrites of both mature cOSNs and mOSNs, resulted in clear immunopositivity ranging from the basal to the apical layers of the olfactory epithelium (Figs. 4a–4d). When the whole olfactory rosette was examined, the OD of control was statistically greater than ODs related to the three Hg^{2+} concentrations. Conversely, in the comparison between the three metal concentrations, only OD for LQ was significantly greater than OD for

https://doi.org/10.1017/S1431927621013763 Published online by Cambridge University Press

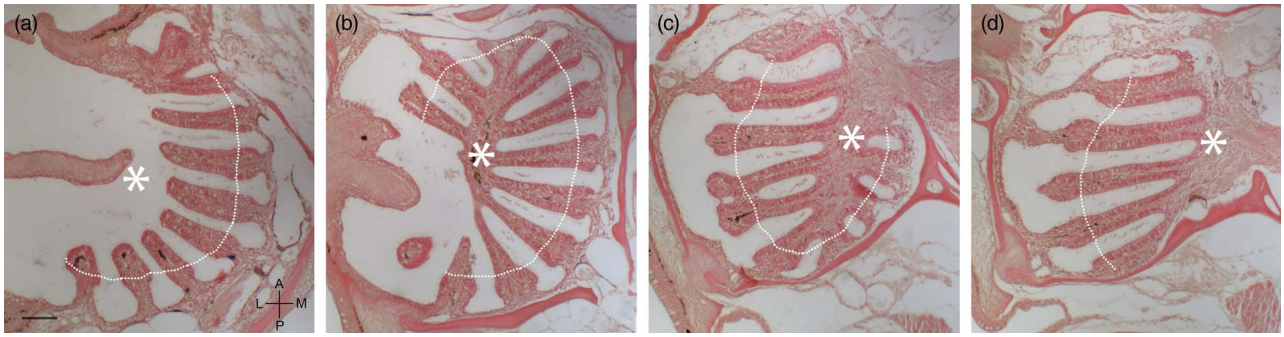

Fig. 1. Morphological analysis of olfactory rosette as it appears in zebrafish head sectioned by frontal planes. (**a–d**) Hematoxylin–eosin-stained semi-serial frontal sections separated by 100 μm at progressively more ventral planes. Asterisks indicate the region of the olfactory rosette examined for PCNA^{+}-cells counting, from the center of the organ to the dotted line representing the border between the sensory and nonsensory subregions. (**a,b**) Lamellae in the dorsal region of the olfactory rosette. (**c,d**) Lamellae in the ventral region of the olfactory rosette. A, anterior; L, lateral; M, medial; P, posterior. Scale bar: 100 μm.

HQ (Fig. 4e). In the dorsal half of the olfactory rosette, OD analysis revealed a condition similar to the whole rosette, with the addition of a significantly higher OD value for MQ compared to HQ (Fig. 4f). In the ventral half of the olfactory rosette, OD resembled what is found in the whole organ (Fig. 4g). Image analysis of calretinin immunostained sections permits to evaluate two additional morphometric parameters in the olfactory lamellae: the thickness of the sensory epithelium and the ratio between sensory and nonsensory epithelium areas. Image analysis of the entire olfactory rosette, as well as of each dorsal and ventral half, showed no significant differences in the ratio sensory/nonsensory areas of the olfactory lamellae among the four groups of fish (Figs. 5a–5c). Regarding the epithelium thickness, the value at HQ appeared significantly decreased compared to control, LQ, and MQ not only in the entire rosette but also in each dorsal and ventral half (Figs. 6a–6c). Moreover, in the whole rosette, the thickness of the MQ group was significantly decreased compared to control (Fig. 6a). In the dorsal half of the olfactory rosette, epithelium thickness of LQ, MQ, and HQ groups appeared significantly lower than in control (Fig. 6b).

At the free surface of the olfactory epithelium, anti-$G_{\alpha\ olf}$ antibody marked apical dendrite endings and cilia of cOSNs (Figs. 7a–7d). When the entire olfactory rosette was evaluated, HQ and MQ showed OD values significantly decreased compared to control and LQ (Fig. 7e). In the dorsal half of the olfactory rosette, OD values repeat the condition found in the entire organ (Fig. 7f). In the ventral half of the olfactory rosette, OD values showed no statistically relevant difference (Fig. 7g).

Anti-TRPC2 antibody-stained dendritic apical knobs and microvilli of mOSNs at the apical region of the sensory epithelium of the olfactory rosettes (Figs. 8a–8d). In the whole olfactory rosette, as well as in both its dorsal and ventral halves, mercury exposure resulted in lower OD values than control (Figs. 8e–8g). In the entire rosette and its dorsal half, OD for HQ was statistically lower than values for both MQ and LC (Figs. 8e, 8f). In the ventral half of the olfactory rosette, OD at HQ was significantly lower than LQ only (Fig. 8g).

Anti-TrkA antibody clearly stained crypt cells, big neurons placed in the olfactory epithelium region close to the olfactory lamella surface (Figs. 9a–9d). In the whole olfactory rosette, crypt cell number for MQ and HQ was lower compared to control and LQ (Fig. 9e). In the dorsal half of the olfactory rosette, both MQ and HQ groups show a crypt cell density significantly smaller than in the LQ group (Fig. 9f). Ventrally, cell density showed a similar situation, with values for MQ and HQ lower than control and progressively decreasing with more severe exposure conditions (Fig. 9g).

Anti-HuC/D antibody, specific for both mature and immature neurons, stained the olfactory epithelium from the basal to the apical layer (Figs. 10a–10d). In the whole rosette, as well as in both its dorsal and ventral halves, no significant change in OD was observed between the four fish groups (Figs. 10e–10g).

In the olfactory lamellae, anti-PCNA stained cells undergoing mitotic events reside specifically in the regions bordering the sensory epithelium and also in its basal layer (Figs. 11a–11d). In the whole rosette, as well as in its dorsal half, exposure to Hg^{2+} showed no significant differences between the four groups of fish (Figs. 11e, 11f). When the statistical analysis was restricted to the ventral half of the rosette, Hg^{2+} exposure resulted in a significant increase of mitotic cell density between HQ and the three other groups in the basal layer of the sensory region, while interlamellar curves and the border between sensory and nonsensory epithelium appeared not to be affected (Fig. 11g).

Discussion

In the olfactory epithelium of zebrafish, the immunohistochemical markers investigated allowed the identification of three main populations of OSNs with differential response to Hg^{2+} ions at different concentrations. In the whole olfactory rosette, the OD of $G_{\alpha\ olf}$, indicative for cOSNs, results significantly reduced compared to control only for MQ (22%) and HQ (30%). When compared to each other, the OD of cOSNs at the three used Hg^{2+} concentrations shows values for MQ and HQ significantly lower than LQ (17 and 26%, respectively), indicative for dose dependency. The response of cOSNs to MQ and HQ exposure results dose-independent since OD differences between MQ and HQ turn out to be statistically nonsignificant. The response of cOSNs appears dose-independent also for Ni^{2+} exposure, as previously reported (Lazzari et al., 2019). When the dorsal and ventral half of the olfactory rosette are separately evaluated after Hg^{2+} exposure, the condition of the OD for the dorsal region resembles the outcome for the entire organ. On the contrary, the ventral region of the olfactory rosette shows no significant differences between the four groups of fish. The reasons, as well as the functional relevance of these regional differences in the olfactory organ, are still unclear and require detailed studies. A hypothesis could involve different dynamics of water circulation inside the

https://doi.org/10.1017/S1431927621013763 Published online by Cambridge University Press

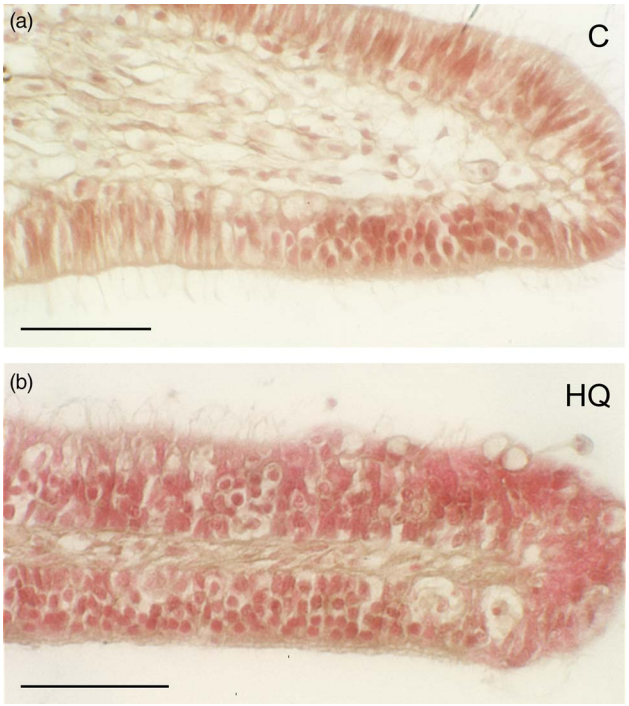

Fig. 2. Olfactory lamellae of zebrafish stained with hematoxylin–eosin. (**a**) Control fish. (**b**) Fish exposed to 200 μg/L Hg^{2+}. Exposure to high mercury concentration caused an increase in the number of unicellular mucous glands opening into the luminal surface of the olfactory lamellae. Olfactory lamellae retain their structural integrity in fish exposed to high mercury concentration. Scale bar = 50 μm.

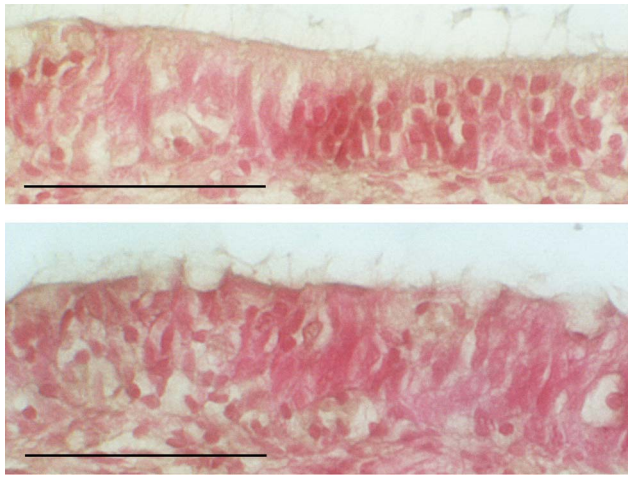

Fig. 3. High magnification images of olfactory lamellae epithelium stained with hematoxylin–eosin. (**a**) Control fish. (**b**) Fish exposed to 200 μg/L Hg^{2+}. Cilia are still present in the epithelium of olfactory lamellae exposed to high mercury concentration. Scale bar = 50 μm.

olfactory chamber, which could differentially expose OSNs to pollutants dissolved in the water. Indeed, in the ventral region of the olfactory rosette, cOSNs could be somehow less exposed to pollutants, as, for example, the water flow entering the olfactory chamber encounters first the lamellae of the dorsal half of the olfactory rosette. Also, different subpopulations of cOSNs, having different sensitivity to Hg^{2+} ions, may be present in different regions of the olfactory organ. By comparing the results on Ni^{2+} and Hg^{2+} exposures, we may suppose that cOSNs have higher Ni^{2+} susceptibility in the ventral zone of the olfactory rosette, whereas Hg^{2+} susceptibility prevails in the dorsal zone (Lazzari et al., 2019). Subpopulations of olfactory neurons appear to exist also in other fish species as in the case of crypt cells in *Poecilia reticulata* (Bettini et al., 2017).

In the whole olfactory rosette after Hg^{2+} exposure, OD for TRPC2, indicative for mOSNs, shows a statistically significant decrease at each metal concentration tested, with a mean value of 49% compared to control. OD values for LQ and MQ are statistically equivalent, but both of them show relevant dose effects compared to HQ. Therefore, similarly to that obtained for $G_{\alpha\ olf}$ (cOSNs), the response for TRPC2 (mOSNs) is greater in the ventral region. The comparison between mean OD values for $G_{\alpha\ olf}$ and TRPC2 suggests that mOSNs are more sensitive to Hg^{2+} exposure than cOSNs. Since, instead, cOSNs are more susceptible than mOSNs when exposed to Cu^{2+} and Ni^{2+} (Lazzari et al., 2017, 2019), this new finding suggests a difference in the response of OSNs to different heavy metals.

Hentig & Byrd-Jacobs (2016) studied the effects of zinc on zebrafish OSNs with both morphological and functional approaches, showing differential impairment of fish OSN classes. In particular, ultrastructural analysis of epithelial surface with scanning electron microscopy showed that cOSNs are heavily affected, whereas mOSNs generally have no or smaller damage. Behavioral findings were in accordance with morphological evidence. In fact, after zinc exposure, the sensibility to amino acids, detected by mOSNs and initiating feeding behavior, was restored more quickly than the response to bile salts, detected by cOSNs and related to social cues. As suggested by Hentig & Byrd-Jacobs (2016), mOSNs may be considered a highly protected component of the olfactory system because they are connected to feeding response and satisfy an immediate need for the individual; instead, cOSNs, that mediate social behavior, may be seen to meet a less urgent necessity for individual survival and may therefore be more subject to damage. Thus, the observed variation can be seen as the outcome of diverse evolutionary forces affecting the OSN populations differently.

Differential impairment of fish OSN classes, even if with opposite findings, was reported applying a functional approach based on electro-olfactograms (EOG) after nickel exposure (Dew et al., 2014). EOG study on fathead minnows (*Pimephales promelas*) and yellow perch (*Perca flavescens*) shows that, in both species, nickel impairs mOSN function whereas there was no significant alteration of cOSN activity. The observed impairment caused by Ni on mOSN function could still represent a success for the individual if it forced fish to swim away from polluted areas in search of food. Based on the above reported functional studies, we may suggest that the preservation of mOSN activity cannot be considered a general feature but can vary after exposure to different metals and/or if considering different fish species.

The results with EOG on nickel exposure of Dew et al. (2014) are in contrast with our findings in zebrafish (Lazzari et al., 2019), since immunohistochemistry revealed that both mOSNs and cOSNs are affected by Ni exposure, with OD reduction for $G_{\alpha\ olf}$ (specific for cOSNs) greater than OD reduction for TRPC2 (specific for mOSNs) (Lazzari et al., 2019). As a possible explanation for the observed difference between immunohistochemical and EOG results, we may suggest that, after metal exposure, OD reduction for each antigen can have a specific threshold beyond which a functional damage occurs. At the concentrations of 0.1 and 0.5 mg/L Ni^{2+} used by Dew et al. (2014) and Lazzari et al. (2019), both $G_{\alpha\ olf}$ and TRPC2 markers show a clear

https://doi.org/10.1017/S1431927621013763 Published online by Cambridge University Press

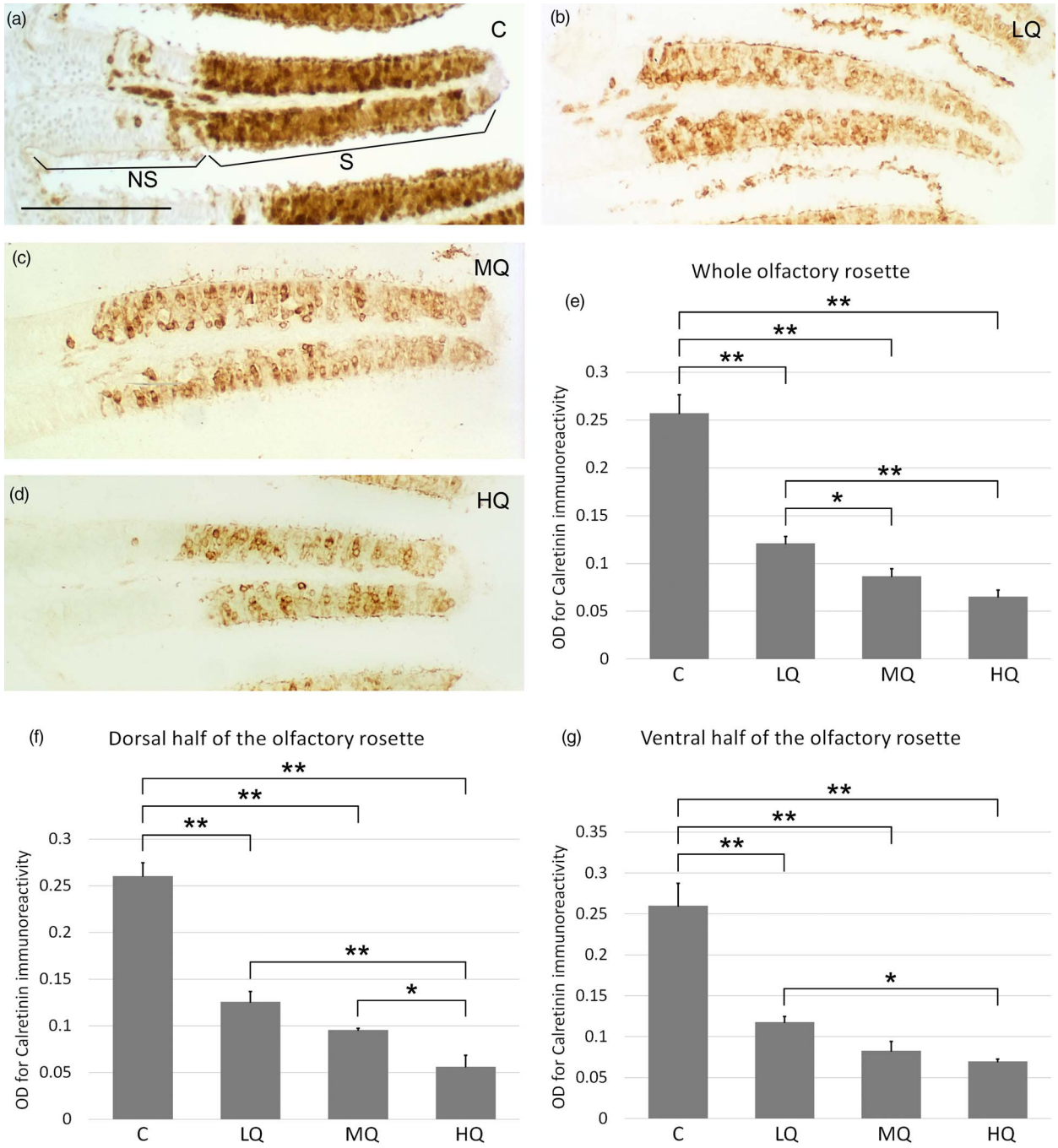

Fig. 4. Calretinin immunohistochemistry in zebrafish olfactory epithelium before and after 50, 100, and 200 μg/L Hg^{2+} exposure. (**a**) Heavy anti-calretinin immunoreaction stains the sensory area (S) of the olfactory lamellae of control fish. The nonsensory region (NS) of the lamellae appears unstained, except for some scattered cells (even if the two areas are well distinguished, there is no barrier between them, so some sensory cells can migrate and differentiate in the adjacent nonsensory region). (**b**) Representative micrograph of lamellae exposed to 50 μg/L of Hg^{2+}. (**c**) Representative micrograph of lamellae exposed to 100 μg/L of Hg^{2+}. (**d**) Representative micrograph of lamellae exposed to 200 μg/L of Hg^{2+}. Scale bar = 50 μm. (**e**) Optical density analysis of the olfactory epithelium in the whole olfactory rosette. (**f**) Optical density analysis of the olfactory epithelium in lamellae of the dorsal half of the olfactory rosette. (**g**) Optical density analysis of the olfactory epithelium covering lamellae of the ventral portion of the olfactory rosette. C, control, 0 μg/L Hg^{2+}; LQ, low quantity, 50 μg/L Hg^{2+}; MQ, medium quantity, 100 μg/L Hg^{2+}; HQ, high quantity, 200 μg/L Hg^{2+}. Asterisks indicate significant differences: *, $p < 0.05$; **, $p < 0.01$.

reduction of their OD values, but, after Ni^{2+} exposure, OD reduction for TRPC2 might exceed its damage-threshold value thus that EOG could indeed reveal alterations in mOSN activities. On the contrary, at the same Ni^{2+} concentrations, the reduction of OD for $G_{\alpha\ olf}$ might remain below its damage-threshold with consequently no effects detected in cOSN functions by EOG.

In immunohistochemical analysis, we reported that cOSNs appear more susceptible to Ni^{2+} than mOSNs because cOSNs have a greater percentage decrease of OD, compared to their control value, than mOSNs. Nevertheless, this percentage shift might be not sufficient to trigger functional alterations in cOSNs. Instead, in mOSNs, a smaller reduction of OD for $G_{\alpha\ olf}$ could

https://doi.org/10.1017/S1431927621013763 Published online by Cambridge University Press

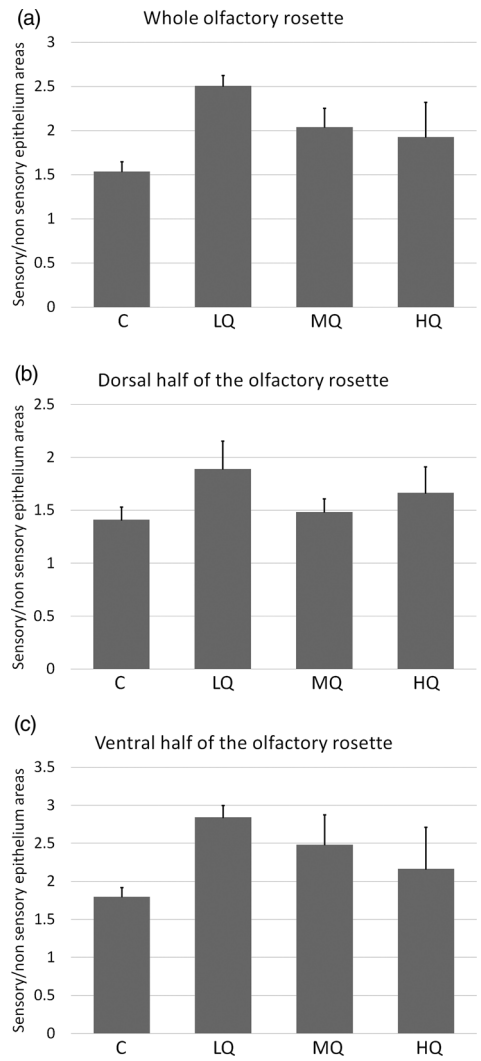

Fig. 5. Ratio between sensory and nonsensory areas of the epithelium covering the lamellae in the olfactory rosette of zebrafish, evaluated by means of the calretinin immunoreactivity before and after 50, 100, and 200 μg/L Hg^{2+} exposure. (**a**) Ratio between sensory and nonsensory areas of the epithelium covering the lamellae in the whole olfactory rosette. (**b**) Ratio between sensory and nonsensory areas of the epithelium overlaying the lamellae in the dorsal half of the olfactory rosette. (**c**) Ratio between nonsensory and sensory areas of the epithelium covering the lamellae in the ventral half of the olfactory rosette. C, control, 0 μg/L Hg^{2+}; LQ, low quantity, 50 μg/L Hg^{2+}; MQ, medium quantity, 100 μg/L Hg^{2+}; HQ, high quantity, 200 μg/L Hg^{2+}.

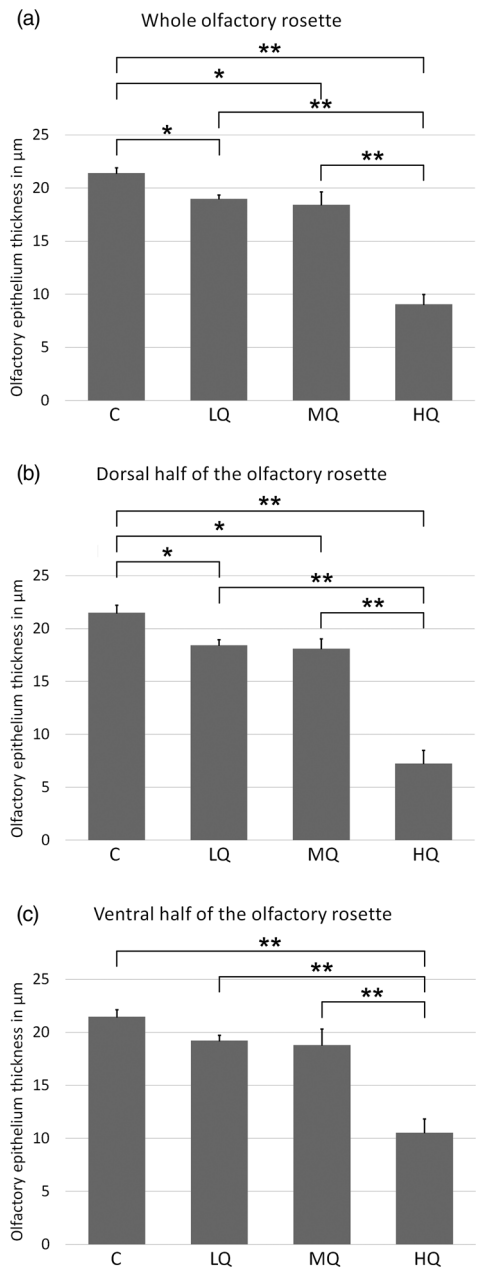

Fig. 6. Sensory epithelium thickness in the zebrafish olfactory epithelium, evaluated by means of calretinin immunoreactivity before and after 50, 100, and 200 μg/L Hg^{2+} exposure. (**a**) Sensory epithelium thickness in the lamellae of the whole olfactory rosette. (**b**) Sensory epithelium thickness in the lamellae of the dorsal region of the olfactory rosette. (**c**) Sensory epithelium thickness in the lamellae of the ventral region of the olfactory rosette. C, control, 0 μg/L Hg^{2+}; LQ, low quantity, 50 μg/L Hg^{2+}; MQ, medium quantity, 100 μg/L Hg^{2+}; HQ, high quantity, 200 μg/L Hg^{2+}. Asterisks indicate significant differences: *, $p < 0.05$; **, $p < 0.01$.

be sufficient to exceed the damage-threshold value and generate functional damage. Interestingly, EOG recordings on copper-exposed fish (Dew et al., 2014) are in accordance with the histological analysis in goldfish (Kolmakov et al., 2009) and zebrafish (Lazzari et al., 2017), with copper specifically affecting cOSNs. Taking all these observations into consideration, we believe that, in studies on metal toxicity, attention must be paid when comparing data obtained with the two types of investigations, since the changes detected by immunohistochemical analysis cannot be always directly compared to functional results. For completeness, it should be mentioned that incongruities among EOG studies also exist (Sandahl et al., 2007; Baldwin et al., 2011). Differences in technical approaches, ions concentrations, exposition times, water chemistry, and intrinsic differences among fish species can explain the discrepancy reported in different electrophysiological investigations (Dew et al., 2012, 2014; Lari et al., 2019).

Another problem concerns the significance of the decrease in immunostaining intensity observed by densitometric analysis at the level of the apical processes of OSNs. This decrement may be indirect evidence of the reduction in the number of OSNs, therefore indicative of cell death. However, OD decrement could also derive from both a reduction in apical process number and a decrease in the expression of the protein chosen as a molecular marker. In the Indian major carp (*Labeo rohita*) exposed to sublethal concentrations of $HgCl_2$, Ghosh & Mandal (2014) analyzed the apical surface of the olfactory epithelium by scanning electron

https://doi.org/10.1017/S1431927621013763 Published online by Cambridge University Press

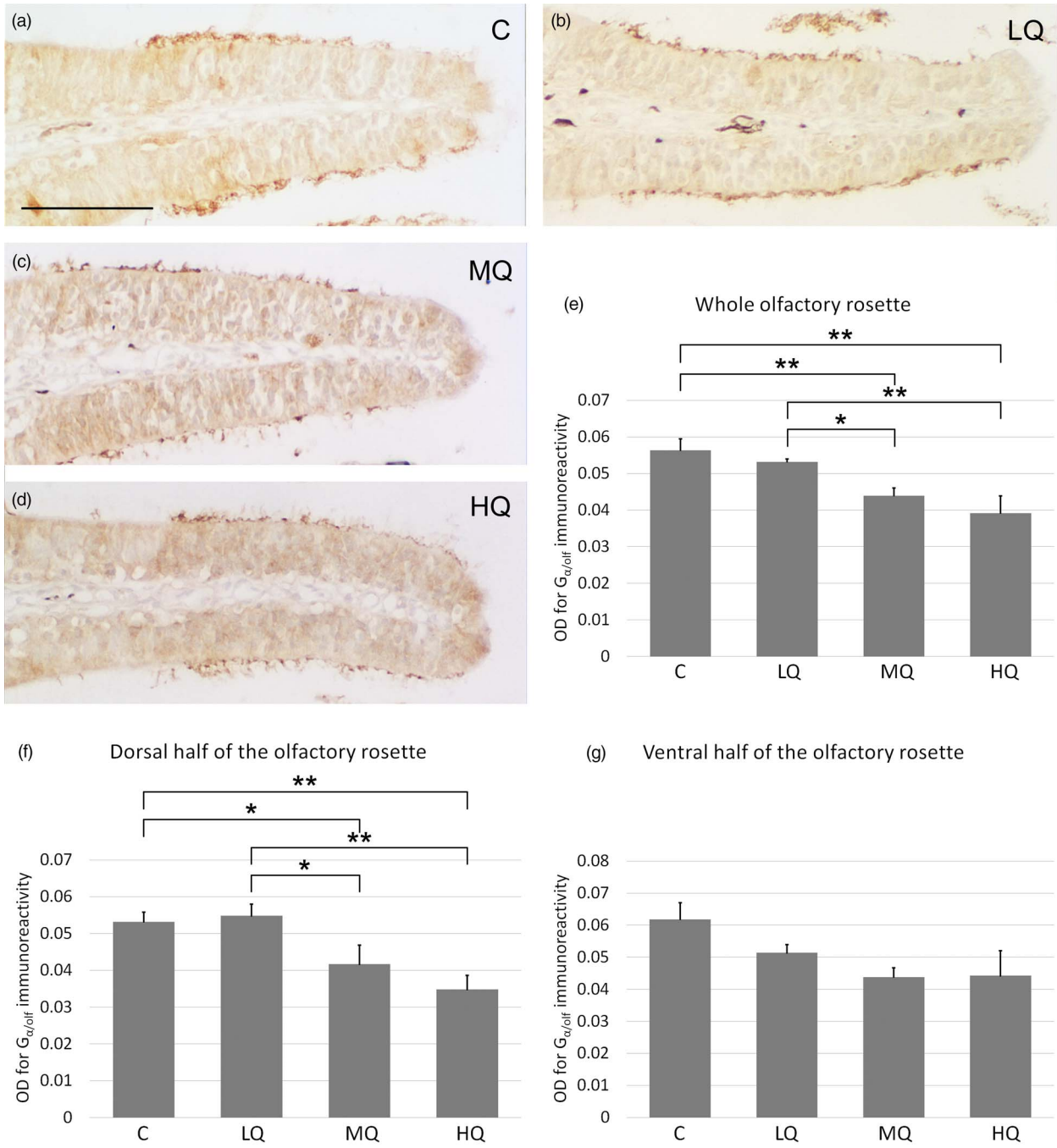

Fig. 7. $G_{\alpha\ olf}$ immunohistochemistry in zebrafish olfactory epithelium before and after 50, 100, and 200 μg/L Hg^{2+} treatment. (**a**) In the olfactory lamellae of control fish, the receptor cell knobs placed in the superficial zone of the sensory epithelium show different $G_{\alpha\ olf}$ immunostaining intensity. (**b**) Representative micrograph of lamellae exposed to 50 μg/L of Hg^{2+}.(**c**) Representative micrograph of lamellae exposed to 100 μg/L of Hg^{2+}. (**d**) Representative micrograph of lamellae exposed to 200 μg/L of Hg^{2+}. Scale bar = 50 μm. (**e**) Optical density analysis of the olfactory epithelium surface in the whole olfactory rosette. (**f**) Optical density analysis of the olfactory epithelium surface in the lamellae of the dorsal area of the olfactory rosette. (**g**) Optical density analysis of the sensory epithelial surface in the lamellae of the ventral area of the olfactory rosette. C, control, 0 μg/L Hg^{2+}; LQ, low quantity, 50 μg/L Hg^{2+}; MQ, medium quantity, 100 μg/L Hg^{2+}; HQ, high quantity, 200 μg/L Hg^{2+}. Asterisks indicate significant differences: *, $p < 0.05$; **, $p < 0.01$.

microscopy. These authors report toxicity responses in fish olfactory epithelium, in particular clumping and loss of cilia. Damage and loss of cilia with retention of microvilli were also described by Ribeiro et al. (1995) in *Trichomycterus brasiliensis* after Hg^{2+} exposure and by Kolmakov et al. (2009) in goldfish after Cu^{2+} treatment. However, ultrastructural studies on zebrafish olfactory epithelium exposed to Hg^{2+} ions are still missing. These morphological studies are important since they could prove whether, also in zebrafish, exposure to mercury leads to cilia and/or microvilli reduction or complete disappearance of apical cell processes with probable cell death. In our immunohistochemical analysis, cell cilia are clearly present and stained in the apical/luminal surface of the olfactory epithelium. Therefore, in zebrafish exposed to the Hg^{2+} concentration tested, a reduction in $G_{\alpha\ olf}$

https://doi.org/10.1017/S1431927621013763 Published online by Cambridge University Press

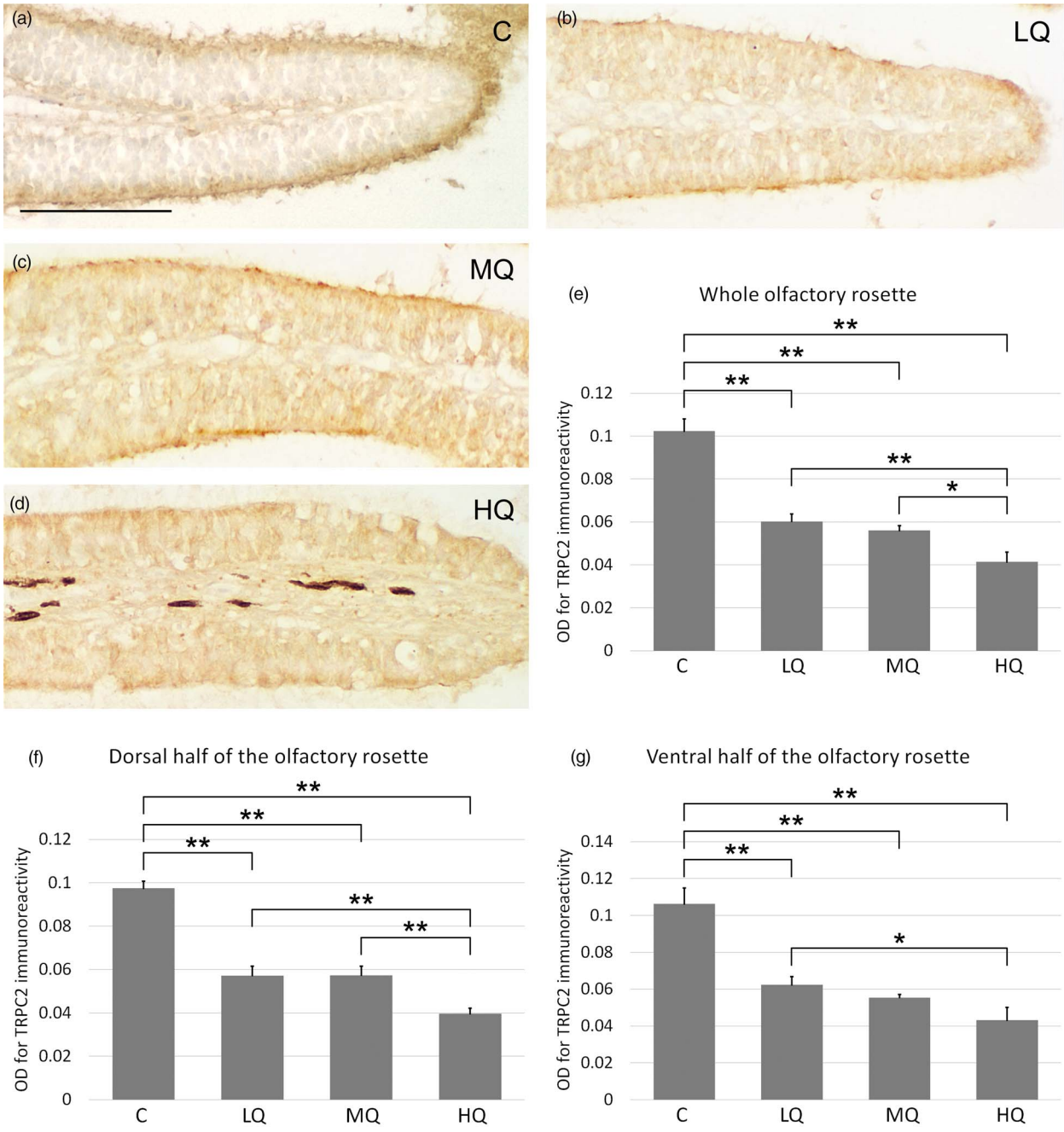

Fig. 8. TRPC2 immunohistochemistry in zebrafish olfactory epithelium before and after 50, 100, and 200 μg/L Hg^{2+} exposure. (**a**) In the sensory areas of the olfactory lamellae of control fish, the apical region of the olfactory epithelium contains the receptor cell endings, which are stained by anti-TRPC2 antibody. (**b**) Representative micrograph of lamellae exposed to 50 μg/L of Hg^{2+}. (**c**) Representative micrograph of lamellae exposed to 100 μg/L of Hg^{2+}. (**d**) Representative micrograph of lamellae exposed to 200 μg/L of Hg^{2+}. Scale bar = 50 μm. (**e**) Optical density analysis of the olfactory epithelium surface in the whole olfactory rosette. (**f**) Optical density analysis of the olfactory epithelium surface in the lamellae of the dorsal half of the olfactory rosette. (**g**) Optical density analysis of the olfactory epithelium surface in the lamellae of the ventral half of the olfactory rosette. C, control, 0 μg/L Hg^{2+}; LQ, low quantity, 50 μg/L Hg^{2+}; MQ, medium quantity, 100 μg/L Hg^{2+}; HQ, high quantity, 200 μg/L Hg^{2+}. Asterisks indicate significant differences: *, $p < 0.05$; **, $p < 0.01$.

and TRPC2 expression could explain the decrement in OD values for these two markers on the still visible apical processes. This hypothesis would be in line with studies reporting that Cu^{2+} exposure could cause epigenetic modifications (Tilton et al., 2008) and down-regulation of transcription of genes involved in olfactory signal transduction (Wang et al., 2013*b*) without morphological damages and cell death. However, since, in the present study, Hg^{2+} exposure is also linked to a reduction in epithelium thickness and cell proliferation activity, we suggest that the reduction in the marker expressions can be in part related to cell death, as we hypothesized in a previous study on Cu^{2+} exposure (Lazzari et al., 2017).

Crypt cells are the third main population of OSNs located in the sensory epithelium covering the olfactory lamellae of fish

https://doi.org/10.1017/S1431927621013763 Published online by Cambridge University Press

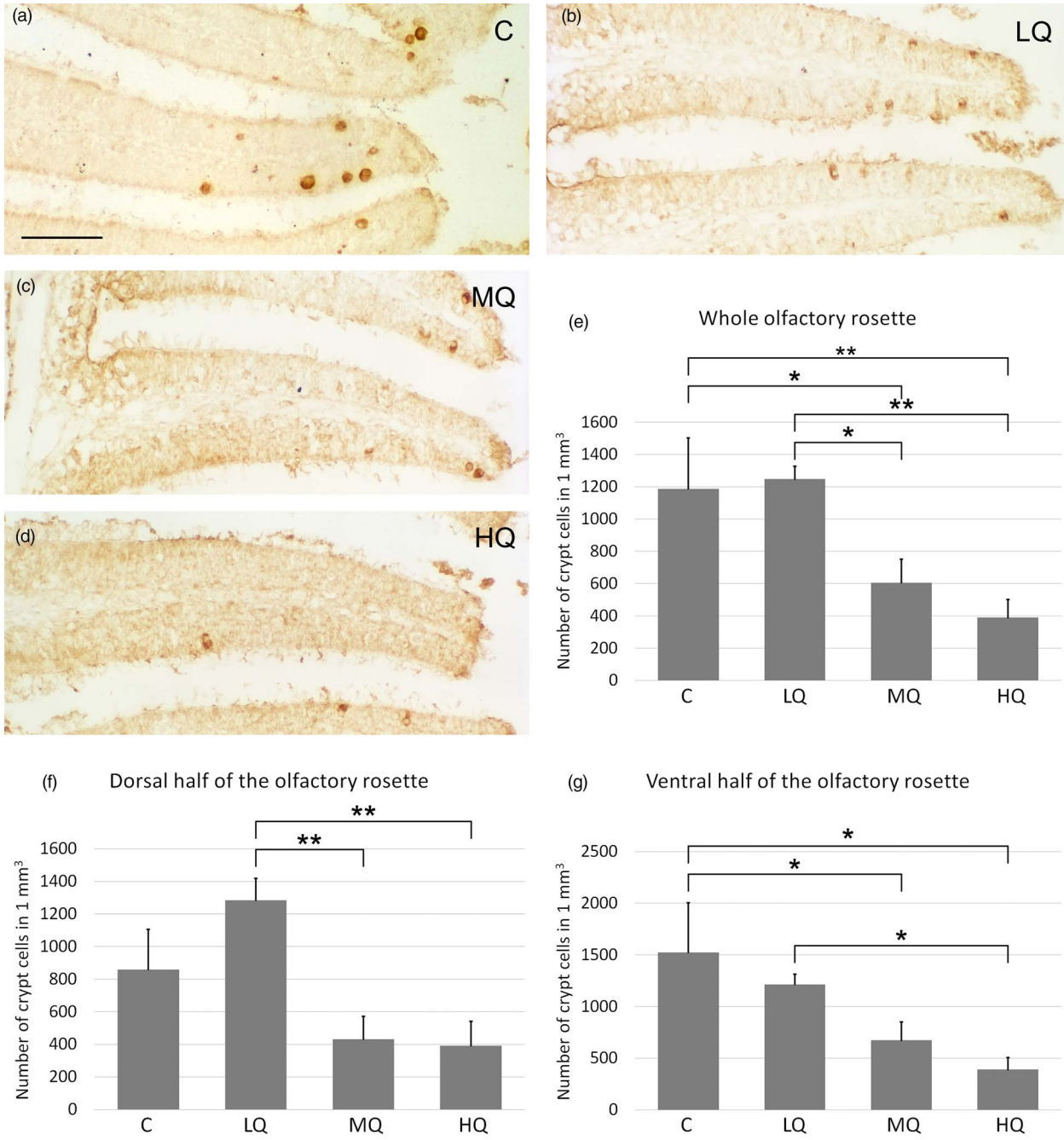

Fig. 9. TrkA immunohistochemistry in zebrafish olfactory epithelium before and after 50, 100, and 200 μg/L Hg^{2+} treatment. (**a**) In olfactory lamellae of control fish, immunostained crypt cells are placed in the superficial layer of the sensory area. (**b**) Representative micrograph of lamellae exposed to 50 μg/L of Hg^{2+}.(**c**) Representative micrograph of lamellae exposed to 100 μg/L of Hg^{2+}. (**d**) Representative micrograph of lamellae exposed to 200 μg/L of Hg^{2+}. Scale bar = 50 μm. (**e**) Density of crypt cells in lamellae of the whole olfactory rosette. (**f**) Density of crypt cells in lamellae of the dorsal region of the olfactory rosette. (**g**) Density of crypt cells in lamellae of the ventral region of the olfactory rosette. C, control, 0 μg/L Hg^{2+}; LQ, low quantity, 50 μg/L Hg^{2+}; MQ, medium quantity, 100 μg/L Hg^{2+}; HQ, high quantity, 200 μg/L Hg^{2+}. Asterisks indicate significant differences: *, $p < 0.05$; **, $p < 0.01$.

olfactory rosette (Hansen & Zeiske, 1998; Hansen & Finger, 2000; Ferrando et al., 2006; Lazzari et al., 2007; Gayoso et al., 2011, 2012). This cell type is not present in the olfactory epithelium of tetrapods. For the localization of crypt cells, TrkA is the molecular marker now recognized as being specific for crypt cells of zebrafish (Catania et al., 2003; Ahuja et al., 2013; Bettini et al., 2016). Therefore, we used anti-TrkA in our studies on the cytological effects of heavy metals on crypt cells (Bettini et al., 2016; Lazzari et al., 2017, 2019, present study). In the whole olfactory rosette, exposure to MQ and HQ Hg^{2+} causes a great decrease in crypt cell density, respectively of 49 and 67% compared to control. In the comparisons between each other, the cell density at the three Hg^{2+} concentrations applied shows values at MQ and HQ statistically lower than LQ (51 and 69%, respectively), indicating dose dependence. Conversely, when MQ and HQ exposure were compared, crypt cell density appears not significantly different,

https://doi.org/10.1017/S1431927621013763 Published online by Cambridge University Press

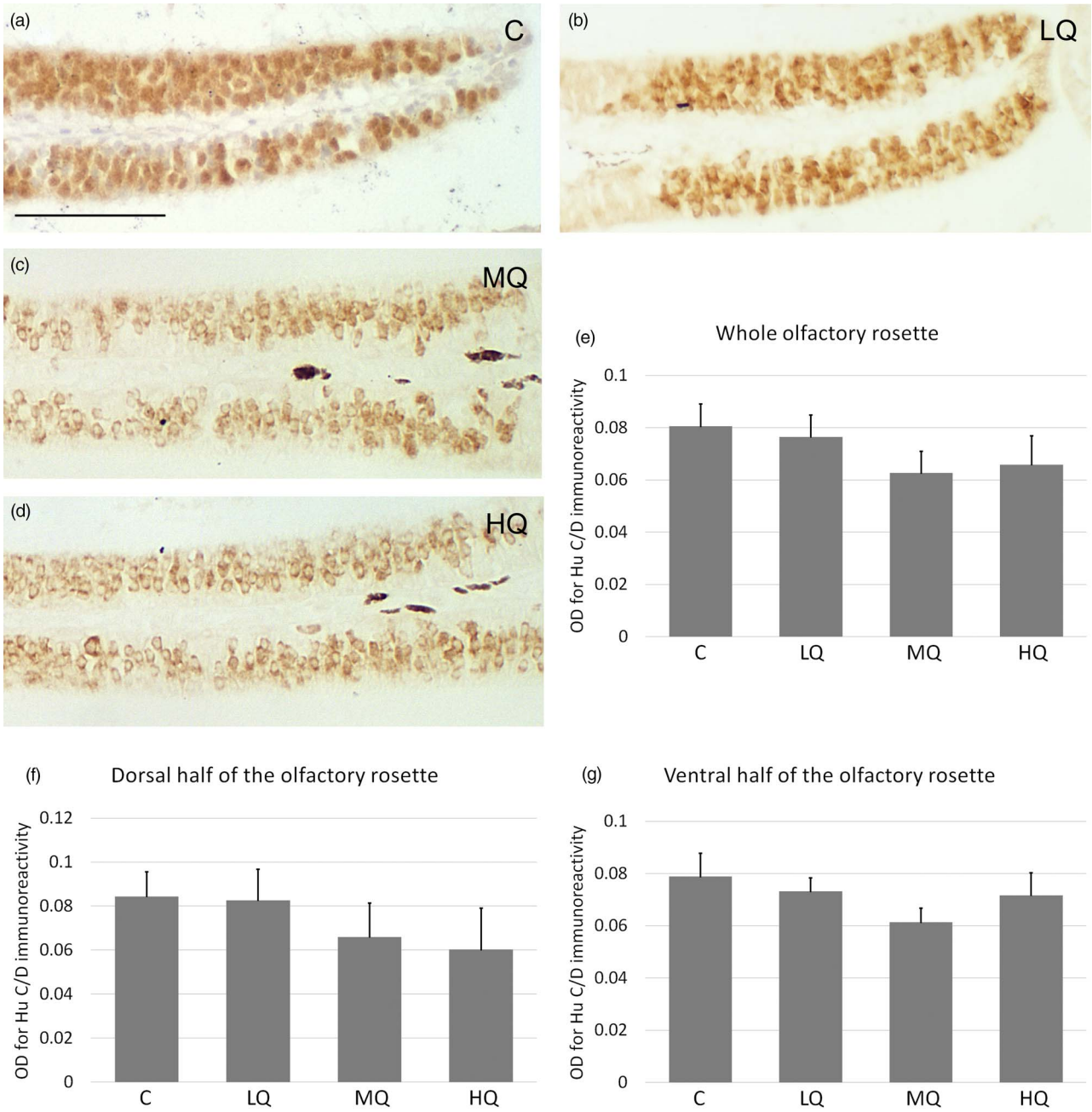

Fig. 10. HuC/D immunohistochemistry in zebrafish olfactory epithelium before and after 50, 100, and 200 μg/L Hg^{2+} exposure. (**a**) In control fish, all the neurons located in the sensory regions of the olfactory lamellae show clear immunopositive cell bodies. (**b**) Representative micrograph of lamellae exposed to 50 μg/L of Hg^{2+}.(**c**) Representative micrograph of lamellae exposed to 100 μg/L of Hg^{2+}. (**d**) Representative micrograph of lamellae exposed to 200 μg/L of Hg^{2+}. Scale bar = 50 μm. (**e**) Optical density analysis of the olfactory epithelium overlaying lamellae in the whole olfactory rosette. (**f**) Optical density analysis of the olfactory epithelium in the dorsal area of the olfactory rosette. (**g**) Optical density analysis of the olfactory epithelium in the ventral area of the olfactory rosette. C, control, 0 μg/L Hg^{2+}; LQ, low quantity, 50 μg/L Hg^{2+}; MQ, medium quantity, 100 μg/L Hg^{2+}; HQ, high quantity, 200 μg/L Hg^{2+}.

thus excluding dose dependence. Mercury concentration between LQ and MQ, and higher than HQ would be useful to investigate the existence of other dose-dependence conditions. When the dorsal and ventral regions of the olfactory rosette are examined separately, Hg^{2+} exposure affects both regions. However, a greater reduction appears in the ventral zone, with crypt cell densities at MQ and HQ of 56 and 75% lower than control, respectively. These density values, even lower than the measures for the whole olfactory rosette, indicate that the ventral half of the olfactory organ is severely affected by Hg^{2+} ions. Previous studies evaluated the response of crypt cells to Cu^{2+} and Ni^{2+} exposures (Lazzari et al., 2017, 2019). In both studies, the statistical analysis does not support any significant difference after metal exposure. Therefore, the conclusion was that Cu^{2+} and Ni^{2+}, at least at the tested concentrations, do not seem to affect crypt cells (Lazzari et al., 2017, 2019). In these studies on Cu^{2+} and Ni^{2+} exposure, the authors hypothesized that the specific morphology of crypt cells can account for the lack of harmful effects on these cells.

https://doi.org/10.1017/S1431927621013763 Published online by Cambridge University Press

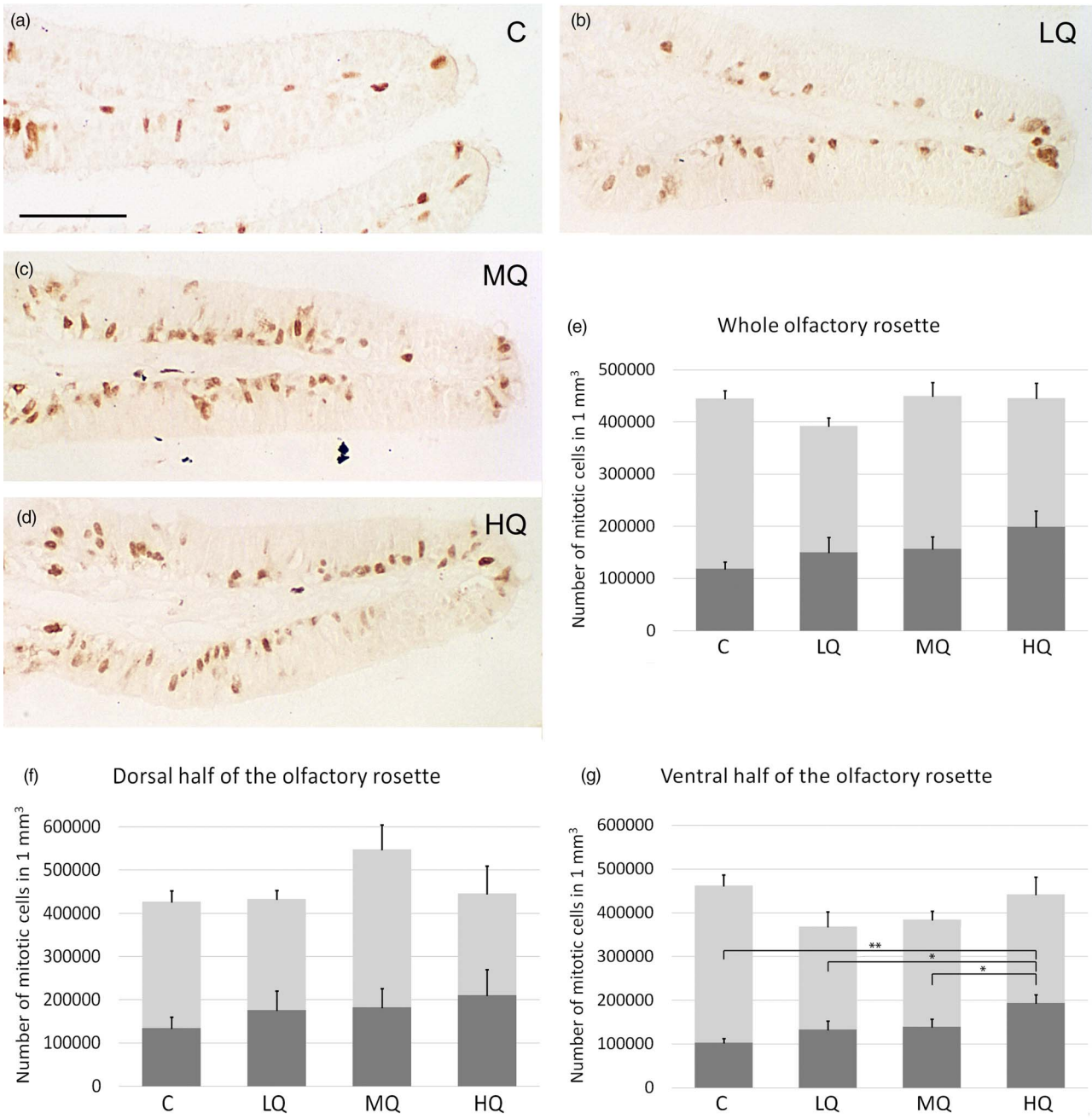

Fig. 11. PCNA immunohistochemistry in zebrafish olfactory epithelium before and after 50, 100, and 200 μg/L Hg^{2+} treatment. (**a**) In olfactory lamellae of control specimen, mitotic cells are visible in the sensory area of the olfactory epithelium. (**b**) Representative micrograph of lamellae exposed to 50 μg/L of Hg^{2+}. (**c**) Representative micrograph of lamellae exposed to 100 μg/L of Hg^{2+}. (**d**) Representative micrograph of lamellae exposed to 200 μg/L of Hg^{2+}. Scale bar = 50 μm. (**e**) Density of dividing cells in the olfactory epithelium covering lamellae in the whole olfactory rosette. Dark gray bars represent the density of $PCNA^{+}$-cells in the basal layer of the olfactory epithelium, while light gray bars represent the density of $PCNA^{+}$-cells in interlamellar curves and the border between sensory and nonsensory regions. (**f**) Density of dividing cells in the olfactory epithelium of the dorsal half of the olfactory rosette. (**g**) Density of dividing cells in the olfactory epithelium of the ventral half of the olfactory rosette. C, control, 0 μg/L Hg^{2+}; LQ, low quantity, 50 μg/L Hg^{2+}; MQ, medium quantity, 100 μg/L Hg^{2+}; HQ, high quantity, 200 μg/L Hg^{2+}. Asterisks indicate significant differences: *, $p < 0.05$; **, $p < 0.01$.

cOSNs and mOSNs have their cilia and microvilli arising from the dendritic apical region of the receptor neurons and are directly exposed to the water flux at the surface of the olfactory epithelium. This condition may account for the great susceptibility of cilia and microvilli to water pollutants. On the contrary, in crypt cells, both cilia and microvilli are present, but not directly immersed in the water flux inside the olfactory chamber (Lazzari et al., 2007). In crypt cells, their cytoplasmic processes are included in a deep cavity at the apical zone of the cell. The narrow crypt hole opening into the olfactory chamber could be responsible for limiting the passage of substances, pollutants included, towards the inner cilia and microvilli. In the present study, a clear effect on crypt cells density could be related to a higher toxicity of mercury compared to copper and nickel.

https://doi.org/10.1017/S1431927621013763 Published online by Cambridge University Press

In vertebrate olfactory epithelium, OSNs have a limited life span. Throughout life, mitotic proliferation takes place in the basal layer of the olfactory epithelium and next cell differentiation gives rise to new neurons substituting dead OSNs (Graziadei & Graziadei, 1979; Bettini et al., 2006*a*). Under normal conditions, OSN populations remain unvaried because mature OSNs downregulate proliferation and differentiation that would substitute deceased elements (Wu et al., 2003). In the olfactory epithelium exposed to Hg^{2+}, the OD for HuC/D, indicative for the total neuronal population including undifferentiated elements, remains statistically constant revealing that substitution of dead cells is still working properly. On the other hand, the density of proliferating cells measured by anti-PCNA immunohistochemistry shows a tendency to increase that becomes statistically relevant only in the ventral half of the olfactory rosette where OD of TRPC2 and TrkA show a significant reduction. These immunohistochemical analyses appear to support each other in suggesting that a certain degree of cell death occurs in the populations of mature OSNs after Hg^{2+} exposure.

Another consideration regards the regions involved in active neurogenesis. Bayramli et al. (2017) and Calvo-Ochoa et al. (2021) reported that the main sites of the proliferation of new olfactory neurons are the interlamellar curve and the sensory/nonsensory border, while the sensory epithelium does not contribute to constitutive cell turnover. mOSNs and cOSNs originate from both marginal sites; nonetheless, cOSNs seem to be prevalently generated in the interlamellar site, while mOSNs in the sensory/nonsensory border (Bayramli et al., 2017). As a consequence, we could expect some density variations in the two parts of the olfactory organ, to regenerate the cOSNs lost in the dorsal rosette and the mOSNs in the ventral one. However, we did not observe a significant difference among treatments in the proliferative activity in these regions, while the increment is statistically evident in the basal layer of the sensory epithelium. Our finding is in line with Calvo-Ochoa et al. (2021), who reported that, under regenerative conditions in response to damage, the horizontal basal cells (HBCs) in the basal layer of the olfactory sensory epithelium, normally dormant, are activated and start proliferating to expand the population of globose basal progenitor cells (GBCs).

We analyzed three types of OSNs that are intermingled in the OE. However, in zebrafish, it is known that different olfactory receptors segregate into distinct spatial subdomains (Weth et al., 1996), and, recently, Ahuja et al. (2018) showed also distinctly different expression zones for some zebrafish V2R-related OlfC receptors. It could be interesting, even if beyond the scope of the present study, to analyze the effects of toxicants on the different subdomains, examining also if the migration of progenitors from the proliferative zones follows different pathways, as observed by Bayramli et al. (2017).

In previous studies on the effects of metal exposure, zebrafish (30 μg/L Cu^{2+}, Lazzari et al., 2017, 0.1, 0.5, and 1 mg/L Ni^{2+}, Lazzari et al., 2019) and *Tilapia mariae* (20 μg/L Cu^{2+}, Bettini et al., 2006*b*) preserved the structure of their olfactory rosettes and olfactory lamellae. Higher Cu^{2+} concentration gave rise to evident alterations in the olfactory epithelium of *T. mariae* (40 μg/L, Bettini et al., 2006*b*) and in goldfish (0.05–6 mM, Kolmakov et al., 2009). At present, information on morphological (histological and ultrastructural) effects of $HgCl_2$ exposure in fish is restricted to Indian major carp, *Labeo rohita* (66 and 132 μg/L for 15 and 30-day exposure, Ghosh & Mandal, 2014). Further histological and ultrastructural studies can add more detailed information about the reaction of zebrafish OSNs to Hg^{2+} exposure. According to Ghosh & Mandal (2014), we found that mercury exposure causes a proliferation and enlargement of round mucous cells in the olfactory epithelium of zebrafish. Most of them are opening to the luminal surface of the epithelium, showing that an enhancement in mucous secretion occurs. Acetylcholine secretion may be responsible for the upregulation of mucous secretion (Inglis et al., 1997). Mucous film over the olfactory epithelium surface has the function of binding odorants and ions involved in the transduction of olfactory signals. However, when the mucous layer becomes excessive, it prevents pollutants from directly contacting the epithelial surface and decreases toxicity effects (Ghosh & Mandal, 2014), and the mucous can also bind and eliminate heavy metals from the system (Ray et al., 2012).

In the olfactory organ of Indian major carp, another manifestation of toxic effect is the significant increase of the olfactory epithelium thickness due to hyperplasia of basal cells and the appearance of vacuoles (Ghosh & Mandal, 2014). At the higher concentration tested (132 μg/L for 30 days), Ghosh & Mandal (2014) found severe decrement of OSNs and tissue alteration with epithelium thickening due to hyperplasia of epithelial basal cells unable to differentiate in new OSNs and cyst formation. In the olfactory epithelium of zebrafish, as indicated by a limited increase in the density of anti-PCNA immunopositive cells, we suggest that mercury exposure affects less the normal cell cycle regulation. In zebrafish, the decrease in the OD for calretinin, which is indicative for a heterogeneous population of mature cOSNs and mOSNs, is in agreement with the decrease in OD for $G_{\alpha\ olf}$ and TRPC2.

Although no specific study is at present available on the effects of Hg^{2+} on nonneuronal cells of the olfactory epithelium, the lack of severe histological alterations throughout tissue appears in favor of a predominant involvement of OSNs, at least at the Hg^{2+} concentration tested. This is in agreement with previous studies on the effect of Cu^{2+} and Ni^{2+} on zebrafish olfactory organs (Lazzari et al., 2017, 2019). As for Ni^{2+} exposure, in contrast to Cu^{2+} treatment, zebrafish olfactory epithelium does not show any increase in sensory area compared to control by the action of Hg^{2+}. Behavioral and electrophysiological studies of Cu^{2+} action in Colorado pikeminnow (*Ptychocheilus lucius*) (Beyers & Farmer, 2001) and fathead minnow (*Pimephales promelas*) (Dew et al., 2012) suggested that sensory area growth was associated with functional recovery. In this respect, new specific studies could clarify existence, extension, and process of neuronal recovery following Hg^{2+} treatment.

In our experiments, according to the sublethal level of the tested concentrations, only HQ exposure caused a fish mortality rate of 10%. This is consistent with a 30–35% death rate at 220 μg/L $HgCl_2$ reported by Ung et al. (2010).

Little is known about the mechanism of olfaction impairment by mercury. Passow et al. (1961) attributed the inhibition of active transport and other cell functions to mercury affinity for sulfhydryl groups on the cell membrane. Following mercury chloride exposure, Richetti et al. (2011) hypothesize a signal transmission impairment through alterations in cholinergic transmission and in the antioxidant competence of nervous tissue.

Conclusions

The immunohistochemical analysis of the olfactory epithelium shows that Hg^{2+} exposure clearly affects the expression pattern of the molecular markers of the different OSN types.

https://doi.org/10.1017/S1431927621013763 Published online by Cambridge University Press

Interestingly, the different OSNs respond differentially to Hg^{2+} exposure at the sublethal concentration tested. In particular, mOSNs are the most susceptible with a mean reduction of TRPC2 OD of 49% compared to control, against a 19% decrease of $G_{\alpha\ olf}$ OD for cOSNs, and a 37% drop of crypt cell density measured by anti-TrkA staining. These variations show some dose-dependent effects, in particular for TRPC2 OD values. Therefore, immunohistochemical analysis differentiates OSNs by Hg^{2+} sensitivity: mOSNs, crypt cells, and cOSNs, going from the most susceptible to the least. These immunohistochemical results differ from studies on fish exposure to other metals, in which cOSNs resulted more susceptible than mOSNs (Kolmakov et al., 2009; Dew et al., 2014; Ghosh & Mandal, 2014; Lazzari et al., 2017, 2019). Moreover, in zebrafish, crypt cells appeared not statistically modified by Cu^{2+} and Ni^{2+} exposures (Lazzari et al., 2017, 2019), whereas the effect of Hg^{2+} on crypt cells is evident also at the lowest concentration.

In zebrafish, Hg^{2+} exposure revealed that cOSNs were more susceptible in the dorsal region, whereas mOSNs were more affected in the ventral area; this is different from the response to Ni^{2+} exposure that was greater in the ventral half of zebrafish olfactory organ for both cOSNs and mOSNs (Lazzari et al., 2019). We can hypothesize that different subpopulations of receptor cells inside each main type of OSNs may be responsible for the detected regional differences. This hypothesis needs further investigation.

Despite the changes in tissue staining described in this study, immunohistochemical methods, *per se*, do not provide information on functional and ecological outcomes of metal exposure. Different functions characterize cOSNs, mOSNs, and crypt cells (Sato & Suzuki, 2001; Hamdani & Døving, 2006; Vielma et al., 2008; Bazáes & Schmachtenberg, 2012; Ahuja et al., 2013; Biechl et al., 2016). Various studies concern behavioral effects resulting from Cu^{2+} exposure (Scott & Sloman, 2004; Tilton et al., 2011; Svecevičius, 2012; Poulsen et al., 2014; Sovová et al., 2014; da Silva Acosta et al., 2016; Simonato et al., 2016) and Ni^{2+} treatment (Dew et al., 2014, 2016). It should also be pointed out that, at present, no molecule acting as a specific activator of crypt cells is known, and this complicates the set up of behavioral investigations for this cell type. Also, when considering the behavioral implications of contaminants on the overall olfactory sensing of fish, we should remember that olfactory function impairment could reasonably derive from a combination of effects of pollutants on OSN types, on sensory integration circuits, and on effector organs (Abu Bakar et al., 2017; Amorim et al., 2017). Further studies analyzing transcriptomic profiles of the olfactory mucosa under different exposure conditions, as well as electro-olfactographic and behavioral effects resulting from mercury exposure, will significantly increase our knowledge about the mechanism of action of this metal in fish olfaction impairment.

Financial support. This work was supported by national public funds grant RFO2017FRANCESCHINI from the Italian Ministry of University and Research (MUR).

Conflicts of interest. The authors declare that they have no conflicts of interest.

References

Abreu MS, Giacomini AC, Kalueff AV & Barcellos LJ (2016). The smell of "anxiety": Behavioral modulation by experimental anosmia in zebrafish. *Physiol Behav* **157**, 67–71.

Abreu MS, Giacomini AC, Rodriguez R, Kalueff AV & Barcellos LJ (2017). Effects of $ZnSO_4$-induced peripheral anosmia on zebrafish behavior and physiology. *Behav Brain Res* **320**, 275–281.

Abu Bakar N, Mohd Sata NS, Ramlan NF, Wan Ibrahim WN, Zulkifli SZ, Che Abdullah CA, Ahmad S & Amal MN (2017). Evaluation of the neurotoxic effects of chronic embryonic exposure with inorganic mercury on motor and anxiety-like responses in zebrafish (*Danio rerio*) larvae. *Neurotoxicol Teratol* **59**, 53–61.

Ahuja G, Ivandić I, Saltürk M, Oka Y, Nadler W & Korsching SI (2013). Zebrafish crypt neurons project to a single, identified mediodorsal glomerulus. *Sci Rep* **3**, 2063.

Ahuja G, Reichel V, Kowatschew D, Syed AS, Kotagiri AK, Oka Y, Weth F & Korsching SI (2018). Overlapping but distinct topology for zebrafish V2R-like olfactory receptors reminiscent of odorant receptor spatial expression zones. *BMC Genomics* **19**, 383–397.

Amorim J, Fernandes M, Vasconcelos V & Teles LO (2017). Evaluation of the sensitivity spectrum of a video tracking system with zebrafish (*Danio rerio*) exposed to five different toxicants. *Environ Sci Pollut Res* **24**, 16086–16096.

Azizishirazi A, Dew WA, Bougas B, Dashtban M, Bernatchez L & Pyle GG (2014). Chemosensory mediated behaviors and gene transcription profiles in wild yellow perch (*Perca flavescens*) from metal contaminated lakes. *Ecotoxicol Environ Saf* **106**, 239–245.

Baldwin DH, Tatara CP & Scholz NL (2011). Copper-induced olfactory toxicity in salmon and steelhead: Extrapolation across species and rearing environments. *Aquat Toxicol* **101**, 295–297.

Bayramli X, Kocagöz Y, Sakizli U & Fuss SH (2017). Patterned arrangements of olfactory receptor gene expression in zebrafish are established by radial movement of specified olfactory sensory neurons. *Sci Rep* **7**, 5572–5588.

Bazáes A & Schmachtenberg O (2012). Odorant tuning of olfactory crypt cells from juvenile and adult rainbow trout. *J Exp Biol* **215**, 1740–1748.

Bernhoft RA (2012). Mercury toxicity and treatment: A review of the literature. *J Environ Public Health* **2012**, 460508.

Bettini S, Ciani F & Franceschini V (2006*a*). Cell proliferation and growth-associated protein 43 expression in the olfactory epithelium in *Poecilia reticulata* after copper solution exposure. *Eur J Histochem* **50**, 141–146.

Bettini S, Ciani F & Franceschini V (2006*b*). Recovery of the olfactory receptor neurons in the African *Tilapia mariae* following exposure to low copper level. *Aquat Toxicol* **76**, 321–328.

Bettini S, Lazzari M, Ferrando S, Gallus L & Franceschini V (2016). Histopathological analysis of the olfactory epithelium of zebrafish (*Danio rerio*) exposed to sublethal doses of urea. *J Anat* **228**, 59–69.

Bettini S, Milani L, Lazzari M, Maurizii MG & Franceschini V (2017). Crypt cell markers in the olfactory organ of *Poecilia reticulata*: Analysis and comparison with the fish model *Danio rerio*. *Brain Struct Funct* **222**, 3063–3074.

Beyers DW & Farmer MS (2001). Effects of copper on olfaction of Colorado pikeminnow. *Environ Toxicol Chem* **20**, 907–912.

Bhan A & Sarkar NN (2005). Mercury in the environment: Effect on health and reproduction. *Rev Environ Health* **20**, 39–56.

Biechl D, Tietje K, Gerlach G & Wullimann MF (2016). Crypt cells are involved in kin recognition in larval zebrafish. *Sci Rep* **6**, 24590.

Bjørklund G, Dadar M, Mutter J & Aaseth J (2017). The toxicology of mercury: Current research and emerging trends. *Environ Res* **159**, 545–554.

Braubach OR, Fine A & Croll RP (2012). Distribution and functional organization of glomeruli in the olfactory bulbs of zebrafish (*Danio rerio*). *J Comp Neurol* **520**, 2317–2339.

Bresch H (1982). Investigation of the long-term action of xenobiotics on fish with special regard to re production. *Ecotoxicol Environ Saf* **6**, 102–112.

Calvo-Ochoa E, Byrd-Jacobs CA & Fuss SH (2021). Diving into the streams and waves of constitutive and regenerative olfactory neurogenesis: Insights from zebrafish. *Cell Tissue Res* **383**, 227–253.

Catania S, Germanà A, Laurà R, Gonzalez-Martinez T, Ciriaco E & Vega JA (2003). The crypt neurons in the olfactory epithelium of the adult zebrafish express TrkA-like immunoreactivity. *Neurosci Lett* **350**, 5–8.

Cruz FF, Leite CE, Pereira TC, Bogo MR, Bonan CD, Battistini AMO, Campos MM & Morrone FB (2013). Assessment of mercury

https://doi.org/10.1017/S1431927621013763 Published online by Cambridge University Press

chloride-induced toxicity and the relevance of P2X7 receptor activation in zebrafish larvae. *Comp Biochem Physiol C Toxicol Pharmacol* **158**, 159–164.

da Silva Acosta D, Danielle NM, Altenhofen S, Luzardo MD, Gomes Costa P, Bianchini A, Bonan CD, Souza da Silva R & Dafre AL (2016). Copper at low levels impairs memory of adult zebrafish (*Danio rerio*) and affects swimming performance of larvae. *Comp Biochem Physiol C Toxicol Pharmacol* **185–186**, 122–130.

Dew WA, Azizishirazi A & Pyle GG (2014). Contaminant-specific targeting of olfactory sensory neuron classes: Connecting neuron class impairment with behavioural deficits. *Chemosphere* **112**, 519–525.

Dew WA, Veldhoen N, Carew AC, Helbing CC & Pyle GG (2016). Cadmium-induced olfactory dysfunction in rainbow trout: Effects of binary and quaternary metal mixtures. *Aquat Toxicol* **172**, 86–94.

Dew WA, Wood CM & Pyle GG (2012). Effects of continuous copper exposure and calcium on the olfactory response of fathead minnows. *Environ Sci Technol* **46**, 9019–9026.

Eisthen HL (1992). Phylogeny of the vomeronasal system and of receptor cell types in the olfactory and vomeronasal epithelia of vertebrates. *Microsc Res Tech* **23**, 1–21.

Ferrando S, Bottaro M, Gallus L, Girosi L, Vacchi M & Tagliafierro G (2006). Observations of crypt neuron-like cells in the olfactory epithelium of a cartilaginous fish. *Neurosci Lett* **403**, 280–282.

Ferrando S, Bottaro M, Gallus L, Girosi L, Vacchi M & Tagliafierro G (2007). First detection of olfactory marker protein (OMP) immunoreactivity in the olfactory epithelium of a cartilaginous fish. *Neurosci Lett* **413**, 173–176.

Ferrando S, Gallus L, Gambardella C, Amaroli A, Vallarino M & Tagliafierro G (2011). Immunolocalization of G protein alpha subunits in the olfactory system of *Polypterus senegalus* (Cladistia, Actinopterygii). *Neurosci Lett* **499**, 127–131.

Fleck JA, Marvin-DiPasquale M, Eagles-Smith CA, Ackerman JT, Lutz MA, Tate M, Alpers CN, Hall BD, Krabbenhoft DP & Eckley CS (2016). Mercury and methylmercury in aquatic sediment across western North America. *Sci Total Environ* **568**, 727–738.

Gayoso JÁ, Castro A, Anadón R & Manso MJ (2011). Differential bulbar and extrabulbar projections of diverse olfactory receptor neuron populations in the adult zebrafish (*Danio rerio*). *J Comp Neurol* **519**, 247–276.

Gayoso J, Castro A, Anadón R & Manso MJ (2012). Crypt cells of the zebrafish *Danio rerio* mainly project to the dorsomedial glomerular field of the olfactory bulb. *Chem Senses* **37**, 357–369.

Germanà A, Paruta S, Germanà GP, Ochoa-Erena FJ, Montalbano G & Vega JA (2007). Differential distribution of S100 protein and calretinin in mechanosensory and chemosensory cells of adult zebrafish (*Danio rerio*). *Brain Res* **1162**, 48–55.

Ghosh D & Mandal DK (2014). Mercuric chloride induced toxicity responses in the olfactory epithelium of *Labeo rohita* (Hamilton): A light and electron microscopy study. *Fish Physiol Biochem* **40**, 83–92.

Goldman LR & Shannon MW (2001). Technical report: Mercury in the environment: Implications for pediatricians. *Pediatrics* **108**, 197–205.

Gonzalez-Raymat H, Liu G, Liriano C, Li Y, Yin Y, Shi J, Jiang G & Cai Y (2017). Elemental mercury: Its unique properties affect its behavior and fate in the environment. *Environ Pollut* **229**, 69–86.

Graziadei PPC & Monti Graziadei GA (1979). Neurogenesis and neuron regeneration in the olfactory system of mammals. I. Morphological aspects of differentiation and structural organization of the olfactory sensory neurons. *J Neurocytol* **8**, 1–18.

Guzzi G & La Porta CA (2008). Molecular mechanisms triggered by mercury. *Toxicology* **244**, 1–12.

Ha E, Basu N, Bose-O'Reilly S, Dórea JG, McSorley E, Sakamoto M & Chan HM (2017). Current progress on understanding the impact of mercury on human health. *Environ Res* **152**, 419–433.

Hamdani EH & Døving KB (2007). The functional organization of the fish olfactory system. *Prog Neurobiol* **82**, 80–86.

Hamdani H & Døving KB (2006). Specific projection of the sensory crypt cells in the olfactory system in crucian carp, *Carassius carassius*. *Chem Senses* **31**, 63–67.

Hansen A & Finger TE (2000). Phyletic distribution of crypt-type olfactory receptor neurons in fishes. *Brain Behav Evol* **55**, 100–110.

Hansen A, Rolen SH, Anderson K, Morita Y, Caprio J & Finger TE (2003). Correlation between olfactory receptor cell type and function in the channel catfish. *J Neurosci* **23**, 9328–9339.

Hansen A & Zeiske E (1998). The peripheral olfactory organ of the zebrafish, *Danio rerio*: An ultrastructural study. *Chem Senses* **23**, 39–48.

Hentig JT & Byrd-Jacobs CA (2016). Exposure to zinc sulfate results in differential effects on olfactory sensory neuron subtypes in adult zebrafish. *Int J Mol Sci* **17**, 1445.

Hill AJ, Teraoka H, Heideman W & Peterson RE (2005). Zebrafish as a model vertebrate for investigating chemical toxicity. *Toxicol Sci* **86**, 6–19.

Inglis SK, Corboz MR, Taylor AE & Ballard ST (1997). In situ visualization of bronchial submucosal glands and their secretory response to acetylcholine. *Am J Physiol* **272**, L203–L210.

Iqbal T & Byrd-Jacobs C (2010). Rapid degeneration and regeneration of the zebrafish olfactory epithelium after Triton X-100 application. *Chem Senses* **35**, 351–361.

Kolmakov NN, Hubbard PC, Lopes O & Canario AV (2009). Effect of acute copper sulfate exposure on olfactory responses to amino acids and pheromones in goldfish (*Carassius auratus*). *Environ Sci Technol* **43**, 8393–8399.

Krabbenhoft DP & Rickert DA (1995). Mercury contamination of aquatic ecosystems. In *Fact Sheet*, US Geological Survey (Ed.), v. **95**, pp. 216–219. Reston (VA): USGS.

Laberge F & Hara TJ (2001). Neurobiology of fish olfaction: A review. *Brain Res Rev* **36**, 46–59.

Lari E, Razmara P, Bogart SJ, Azizishirazi A & Pyle GG (2019). An epithelium is not just an epithelium: Effects of Na, Cl, and pH on olfaction and/or copper-induced olfactory deficits. *Chemosphere* **216**, 117–123.

Lazzari M, Bettini S, Ciani F & Franceschini V (2007). Light and transmission electron microscopy study of the peripheral olfactory organ of the guppy, *Poecilia reticulata* (Teleostei Poecilidae). *Microsc Res Tech* **70**, 782–789.

Lazzari M, Bettini S, Milani L, Maurizii MG & Franceschini V (2017). Differential response of olfactory sensory neuron populations to copper ion exposure in zebrafish. *Aquat Toxicol* **183**, 54–62.

Lazzari M, Bettini S, Milani L, Maurizii MG & Franceschini V (2019). Differential nickel-induced responses of olfactory sensory neuron populations in zebrafish. *Aquat Toxicol* **206**, 14–23.

Macirella R, Guardia A, Pellegrino D, Bernabò I, Tronci V, Ebbesson LOE, Sesti S, Tripepi S & Brunelli E (2016). Effects of two sublethal concentrations of mercury chloride on the morphology and metallothionein activity in the Liver of Zebrafish (Danio rerio). *Int J Mol Sci* **17**, 361.

McIntyre JK, Baldwi DH, Meador JP & Scholz NL (2008). Chemosensory deprivation in juvenile coho salmon exposed to dissolved copper under varying water chemistry conditions. *Environ Sci Technol* **42**, 1352–1358.

McIntyre JK, Baldwin DH, Beauchamp DA & Scholz NL (2012). Low-level copper exposures increase visibility and vulnerability of juvenile coho salmon to cutthroat trout predators. *Ecol Appl* **22**, 1460–1471.

Passow H, Rothstein A & Clarkson TW (1961). The general pharmacology of the heavy metals. *Pharmacol Rev* **13**, 185–224.

Poulsen SB, Svendsen JC, Aarestrup K & Malte H (2014). Calcium-dependent behavioural responses to acute copper exposure in *Oncorhynchus mykiss*. *J Fish Biol* **84**, 1326–1339.

Ray D, Ghosh D & Mandal DK (2012). Induction of metallothionein in the olfactory epithelium of *Channa punctatus* (Bloch) in response to cadmium exposure: An immunohistochemical study. *Proc Zool Soc* **65**, 40–44.

Razmara P, Imbery JJ, Koide E, Helbing CC, Wiseman SB, Gauthier PT, Bray DF, Needham M, Haight T, Zovoilis A & Pyle GG (2021). Mechanism of copper nanoparticle toxicity in rainbow trout olfactory mucosa. *Environ Pollut* **284**, 117141.

Ribeiro CA, Fernandes LM, Carvalho CS, Cardoso RI & Turcatti NM (1995). Acute effects of mercuric chloride on the olfactory epithelium of *Trichomycterus brasiliensis*. *Ecotoxicol Environ Saf* **31**, 104–109.

Richetti S, Rosemberg D, Ventura-Lima J, Monserrat J, Bogo M & Bonan C (2011). Acetylcholinesterase activity and antioxidant capacity of zebrafish brain is altered by heavy metal exposure. *Neurotoxicology* **32**, 116–122.

Risher JF & De Rosa CT (2007). Inorganic: The other mercury. *J Environ Health* **70**, 9–16.

https://doi.org/10.1017/S1431927621013763 Published online by Cambridge University Press

Sandahl JF, Baldwin DH, Jenkins JJ & Scholz NL (2007). A sensory system at the interface between urban stormwater runoff and salmon survival. *Environ Sci Technol* **41**, 2998–3004.

Sato K & Suzuki N (2001). Whole-cell response characteristics of ciliated and microvillous olfactory receptor neurons to amino acids, pheromone candidates and urine in rainbow trout. *Chem Senses* **26**, 1145–1156.

Scott GR & Sloman KA (2004). The effects of environmental pollutants on complex fish behaviour: Integrating behavioural and physiological indicators of toxicity. *Aquat Toxicol* **68**, 369–392.

Scott GR, Sloman KA, Rouleau C & Wood CM (2003). Cadmium disrupts behavioural and physiological responses to alarm substance in juvenile rainbow trout (*Oncorhynchus mykiss*). *J Exp Biol* **206**, 1779–1790.

Simonato JD, Mela M, Doria HB, Guiloski IC, Randi MA, Carvalho PS, Meletti PC, Silva de Assis HC, Bianchini A & Martinez CB (2016). Biomarkers of waterborne copper exposure in the neotropical fish *Prochilodus lineatus*. *Aquat Toxicol* **170**, 31–41.

Sorensen PW & Caprio J (1998). Chemoreception in fish. In *The Physiology of Fishes*, Evans RE (Ed.), pp. 375–405. Boca Raton, FL: CRC Press.

Sovová T, Boyle D, Sloman KA, Vanegas Pérez C & Handy RD (2014). Impaired behavioural response to alarm substance in rainbow troutexposed to copper nanoparticles. *Aquat Toxicol* **152**, 195–204.

Sun Y, Li Y, Liu Z & Chen Q (2018). Environmentally relevant concentrations of mercury exposure alter thyroid hormone levels and gene expression in the hypothalamic–pituitary–thyroid axis of zebrafish larvae. *Fish Physiol Biochem* **44**, 1175–1183.

Svecevičius G (2012). Avoidance of copper and zinc by rainbow trout *Oncorhynchus mykiss* pre-exposed to copper. *Bull Environ Contam Toxicol* **88**, 1–5.

Syversen T & Kaur P (2012). The toxicology of mercury and its compounds. *J Trace Elem Med Biol* **26**, 215–226.

Tierney KB, Baldwin DH, Hara TJ, Ross PS, Scholz NL & Kennedy CJ (2010). Olfactory toxicity in fishes. *Aquat Toxicol* **96**, 2–26.

Tilton FA, Bammler TK & Gallagher EP (2011). Swimming impairment and acetylcholinesterase inhibition in zebrafish exposed to copper or chlorpyrifos separately, or as mixtures. *Comp Biochem Physiol C Toxicol Pharmacol* **153**, 9–16.

Tilton F, Tilton SC, Bammler TK, Beyer R, Farin F, Stapleton PL & Gallagher EP (2008). Transcriptional biomarkers and mechanisms of copper-induced olfactory injury in zebrafish. *Environ Sci Technol* **42**, 9404–9411.

Ung CY, Lam SH, Hlaing MM, Winata CL, Korzh S, Mathavan S & Gong Z (2010). Mercury-induced hepatotoxicity in zebrafish: In vivo mechanistic insights from transcriptome analysis, phenotype anchoring and targeted gene expression validation. *BMC Genomics* **11**, 212.

Vielma A, Ardiles A, Delgado L & Schmachtenberg O (2008). The elusive crypt olfactory receptor neuron: Evidence for its stimulation by amino acids and cAMP pathway agonists. *J Exp Biol* **211**, 2417–2422.

Vutukuru SS & Basani K (2013). Acute effects of mercuric chloride on glycogen and protein content of zebra fish, *Danio rerio*. *J Environ Biol* **34**, 277–281.

Wang H, Liang Y, Li S & Chang J (2013*a*). Acute toxicity, respiratory reaction, and sensitivity of three cyprinid fish species caused by exposure to four heavy metals. *PLoS One* **8**, e65282.

Wang L, Bammler TK, Beyer RP & Gallagher EP (2013*b*). Copper-induced deregulation of microRNA expression in the zebrafish olfactory system. *Environ Sci Technol* **47**, 7466–7474.

Weth F, Nadler W & Korsching S (1996). Nested expression domains for odorant receptors in zebrafish olfactory epithelium. *Proc Natl Acad Sci USA* **93**, 13321–13326.

Wu HH, Ivkovie S, Murray RC, Jaramillo S, Lyons KM, Johnson JE & Calof AE (2003). Autoregulation of neurogenesis by GDF11. *Neuron* **37**, 197–207.

Zhu S, Zhang Z & Žagar D (2018). Mercury transport and fate models in aquatic systems: A review and synthesis. *Sci Total Environ* **639**, 538–549.

Zielinski BS & Hara TJ (2006). Olfaction. In *Fish Physiology: Sensory Systems Neuroscience*, Hara TJ & Zielinski BS (Eds.), vol. **25**, pp. 1–43. San Diego: Elsevier.

https://doi.org/10.1017/S1431927621013763 Published online by Cambridge University Press